

Received July 22, 2020, accepted August 1, 2020, date of publication August 6, 2020, date of current version August 20, 2020.

Digital Object Identifier 10.1109/ACCESS.2020.3014726

A Novel Method to Actively Damp the Vibration of the Hybrid Powertrain by Utilizing a Flywheel Integrated-Starter-Generator

YAODONG HU¹, FUYUAN YANG^{1,2}, LEI DU¹, JINYU ZHANG¹, AND MINGGAO OUYANG¹

¹State Key Laboratory of Automotive Safety and Energy, Department of Automotive Engineering, Tsinghua University, Beijing 100084, China

²Collaborative Innovation Center of Electric Vehicles in Beijing, Beijing 100081, China

Corresponding author: Fuyuan Yang (fyyang@tsinghua.edu.cn)

This work was supported in part by the National Key Research and Development Program of China under Contract 2017YFB0103502, and in part by the International Science and Technology Cooperation Program of China under Contract 2017YFE0102800.

ABSTRACT In this paper, a novel method to actively damp the powertrain vibration by utilizing a flywheel integrated starter generator (FISG) is proposed and validated on the testbench. A more light-weighted, economical, and compact hybrid powertrain devoid of clutches or dampers is built by replacing its flywheel with the ISG rotor. Motor torque having the opposite phase of the engine torque is applied to reduce the vibration. As opposed to the passive methods, which usually make use of the inertial and/or the damping properties of the components to absorb the vibration, this active approach is defined as active damping. Firstly, active damping is proved to be theoretically feasible by simulation based on an engine torque observer. To get the practical-application-oriented motor torque waveform, the observer torque is then processed by considering some realistic factors, such as the motor's response delay and the torque demand limit at MCU (Motor Control Unit), and is finally simplified as the rectangular waveform by off-line simulation. Secondly, an algorithm operating on the original resolver aimed at calculating the real-time crank position is proposed and programmed directly in the MCU. Finally, active damping is realized online utilizing a feedforward method by programming the crank-torque table in MCU. Experiments in both stable and transient conditions are conducted. Results show that active damping can attenuate the vibration effectively, especially over low speed and load ranges. The speed fluctuation range and the cyclic squared angular acceleration can be reduced by 79.7% and 89.7% respectively at 700 rpm when cranking. The crank vibration in transient conditions, including dragging and free deceleration, can also be suppressed, showing potential to realize fast and quiet engine start and halt.


INDEX TERMS Active damping, crank position calculation, engine torque cancellation, flywheel ISG, hybrid powertrain.

I. INTRODUCTION

Energy saving and emission reduction are becoming two of the most urgent tasks for the global automotive industry. Hybrid technology is one of the most attractive and intensively investigated topics for researchers worldwide [1]–[4]. However, hybrid vehicles have their common and unique NVH (noise, vibration, and harshness) problems. And the driver's attention to the vehicle's NVH performance is comparable to its fuel consumption. Besides, the customer's perception of the vehicle quality closely parallels

its NVH characteristic. Therefore, NVH refinement is an important aspect of powertrain development and vehicle integration [5].

For common internal combustion engines, the periodic fuel combustion in cylinders and the masses of the oscillating moving parts result in pulsing engine torque, which leads to rotational speed fluctuation in crankshaft [6]. Additionally, the torque ripples on the crankshaft may cause the rolling vibration of the engine block. This vibration is then transmitted to the chassis through the engine mounts, affecting the powertrain life span, causing increased noise and vibration, and reducing the drivers' comfort [7]. One method to reduce the rotational speed variation is to increase the crankshaft

The associate editor coordinating the review of this manuscript and approving it for publication was Shiwei Xia .

moment of inertia by installing a flywheel to the end of the crankshaft. Since this method is not able to directly reduce the pulsing engine torque, the vibration on the powertrain can't be damped in the most effective way. More specifically, it acts as a low-pass filter, which would be more effective at higher engine speed. Besides, the powertrain vibration can also be suppressed by the front damper mass, which, however, only reduces vibration at the specific frequency while causes a new resonance frequency at the same time, making it difficult to determine its appropriate damping characteristic. Both methods will put on extra weight on the vehicle, resulting in additional fuel consumption. In a hybrid powertrain, the usage of the electric motor to actively damp the engine torsional vibration should be explored. In such scenario, motor torque having the opposite phase of the engine torque is applied, so that the torsional excitation of the driveline can be minimized. For the implementation of active damping control (ADC), the crankshaft position must be known and a good understanding of the engine torque is mandatory [5].

The concept of using motor to actively damp the vibration has been investigated by many research groups worldwide. This concept was firstly applied to suppress vibration in the rolling piston type compressor in the air conditioner by utilizing an alternator [8], [9]. This concept was then re-adopted by Yuzo Kadomukai at Hitachi to reduce the vehicle idling vibration caused by the engine torque pulses from the individual cylinder combustion by using a motor generator instead of an alternator based on the repetitive learning control algorithm [10]. The results were impressive but the mechanical system in this research was complex with a flywheel mounted to the crankshaft. A microcomputer and extra crank position sensors were also required. In [11], researchers from Nissan Motor used a simple feedforward method to suppress the engine speed variation and the engine block rolling vibration with motor connected directly to the crankshaft end of a four-cylinder gasoline engine. Various insights were obtained with regards to using different motor torque waveforms that could help to reduce the motor size and the energy loss.

The concept of active flywheel was firstly proposed in [12]. This concept was programmed on Matlab, aimed at improving the uniformity of the engine's rotational speed in parallel with lowering the engine weight. This system was also named as ISAD (integrated starter-alternator-damper) [13] in the same year. Subsequent researches were conducted by the Ford Motor Company and Roy I. Davis over the next few years. The term active damping of the engine crankshaft oscillation was firstly proposed and proved to be effective based on the learning control scheme by simulation in research [14]. The scheme compromised a linear feedback controller and a learning feedforward term which could predict the engine torque. This algorithm was finally validated online on a 2.0 L diesel engine [15], in which the controller utilized a classical idea for periodic disturbance attenuation by increasing the open loop gain over the frequency range of the engine pulsations while preserving a reasonable system phase margin. However, the effectiveness of this algorithm was limited by

the quality of the speed sensor, which at higher gains would result in audible noises. In [16] and [17], a control system combining an observer-based high-fidelity wide-bandwidth engine torque feedforward term and an engine speed feedback term was adopted for the active cancellation of the torque ripples on a four-cylinder direct injection diesel engine. The experimental results were impressive. However, a feedback controller operating on the crank speed signal as well as an extra encoder with high resolution for the field-oriented starter alternator control were necessary for its online implementation. Besides, the motor was significantly overdriven, which may harm its life span. Patrick Coirault's research group at Poitiers University also did a series of continuous researches on active damping. Their control strategy to use a motor acting separately on various harmonics of the engine speed was simulated in [18] and validated in [19] on a mono-cylinder diesel engine. This algorithm ensured partial or complete attenuation of each harmonic but could only work at constant speed. Therefore, an oversized flywheel was necessary to add extra inertia to the crankshaft to ensure constant speed. This algorithm had been improved by using the LPV (linear parameter varying) control method for conditions where the engine speed varies. The simulation and experimental results can be found in [20] and [21] separately. The suitability of the LPV control for the engine torque ripples reduction was demonstrated through the torque control implementation of a PMSM (permanent magnet synchronous motor). Experimental results on the same test bench showed that, for the first and the second orders of the engine speed, their amplitudes could be reduced significantly. While the speed fluctuation range, however, could not be suppressed effectively with only the low order harmonics attenuated. In fact, the amplitudes of the higher order harmonics were even larger with this method. This problem might be even more severe for applications on the engine with multiple cylinders. Besides, the experimental driveline was complex. An extra hardware called dynamic-output feedback controller as well as a flywheel were needed. In other researches such as [22] and [23], a new active damping method employing the Harmonic Activation Neural Network was simulated to discuss on the boundaries of this concept due to the limited power of the motor. In [24], a 2 degree-of-freedom controller structure was adopted for the integration of the MPC (model predictive control)-based vibration controller with the MCU (motor control unit). Simulation analysis of the proposed approach under stationary and dynamic operating conditions was discussed focusing on its stationary and dynamic performance and the time variant constraint handling.

Currently, active damping is online applied with high-resolution sensors installed on the crank or extra control units added in the control system, making the prototype much more complex. In this paper, the testbench is simplified by removing the flywheel and connecting the crank and the motor rotor rigidly. Also, the torque to actively damp the vibration can be programmed directly into MCU, so that no additional sensors or controllers are necessary for its final online application.

The overall hybrid system in this paper can be more light-weighted, more compact, and more economical with better comfort.

II. METHODOLOGY AND NOVELTY

In this paper, motor torque having the opposite phase of the engine torque is applied to actively damp the rotational speed fluctuation of the hybrid driveline due to the pulsing engine torque caused by the periodic fuel combustion in cylinders and the masses of the oscillating moving parts. The overall methodology of active damping is show in Fig. 1.

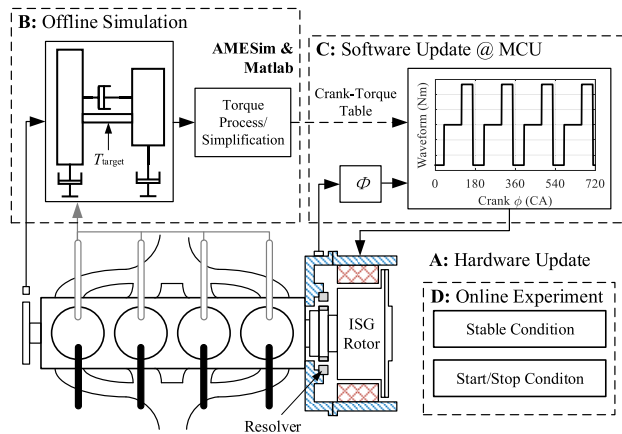


FIGURE 1. The methodology of active damping.

The engine and the motor are mounted rigidly by removing the flywheel and replacing it with the ISG (integrated starter generator) rotor, namely FISG (flywheel ISG). Resolver is a necessary component in the common motor control system. The resolver stator is installed around the inside surface of the flywheel shell. Whereas, its rotor is mounted to the end of the motor rotor, so that the resolver rotor and the stator can be ensured in the same plane. Then, a lumped-mass model of the whole testbench is established to calculate the engine-out torque T_{target} , which is also the torque on the connecting shaft between the engine and the ISG. Next, by considering some realistic factors, the calculated engine-out torque is then processed and simplified to get the online-application-oriented motor torque demand. In a hybrid powertrain, the engine usually works in stable operating conditions. Besides, its periodic and highly crank-position-related torque waveform makes it feasible to calculate offline with the help of the advanced simulation platform. Therefore, active damping can be accomplished by simply adding a feedforward torque control procedure at MCU for applying such opposite-phase engine torque in synchronization with the crank angle. No real-time engine torque observer is needed in the control system. The feasibility of active damping and the reasonability of the engine torque waveform simplification are verified using simulation method, where active damping with different torque strategies, including the phase-inversed engine-out torque waveform and the feedforward method using the simplified torque waveform (rectangular waveform),

are compared. In this paper, the feedforward method is adopted for the final online application. The simplified opposite-phase engine torque is programmed in the MCU as the crank-torque map. The real-time motor torque demand can be determined by looking up the crank-torque table with current crank position. The crank position should be accurate and be obtained real-time. Therefore, a crank online calculation method is developed based on the motor's original resolver. This algorithm is also programmed in MCU. Finally, experiments are conducted in both stationary and transient operating conditions. For transient condition, dragging and free deceleration are tested, which are typical working conditions for a hybrid powertrain.

In this paper, the engine and the motor are integrated by connecting crank and the motor rotor rigidly. No clutches and dampers are needed, making the hybrid powertrain more compact and light-weighted. Also, the engine-out torque can be calculated and simplified offline, so that no engine torque observer is needed in the real-time control system. The crank-torque table can be programmed directly into MCU. Therefore, no additional sensors, computational units or controllers are necessary for its online application. Sensors are only needed when calculating the engine torque and for experimental verification purposes. In conclusion, the overall hybrid system has the potential to be more light-weighted, more compact, and more economical without sacrificing its comfort.

Following the Methodology and Novelty section, section III describes the necessary hardware update for tasks including engine torque calculation and the online application of active damping. In section IV, simulation studies are conducted based on a dual-lumped-mass testbench model. In this part, the feasibility of active damping under different torque strategies are validated and their simulation results are compared. In section V, a novel crank position real-time calculation algorithm based on the original resolver is proposed and online demonstrated. Before the conclusion and the outlook section, section VI presents the experimental results obtained in both stationary and transient working conditions.

III. EXPERIMENTAL SETUP

A. THE OVERALL TESTBENCH

Fig. 2. shows the overall testbench. To make room for the strain sensor and the encoder, the motor rotor is moved coaxially by a distance. Here between the engine and the motor installs an extended ISG shaft. Thereby, the resolver rotor is moved from the motor rotor to the engine-side extended ISG shaft end, whereas on the shaft's motor side installs an encoder. Around the ISG extended shaft, a housing connecting the flywheel shell and the motor stator is designed for supporting purpose. There is also a strain sensor attached to the output shaft. The controllers shown in Fig. 2 are self-developed but typical controllers with nothing particularly special compared with their original ones.

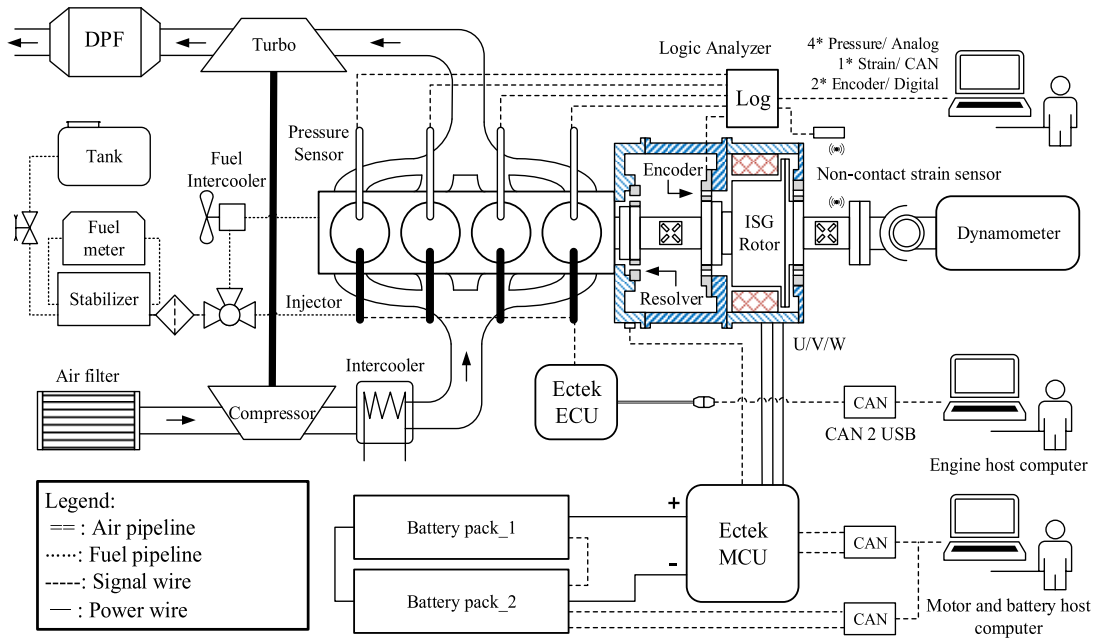


FIGURE 2. The overall testbench.

The self-developed ones are adopted, for no access authority can be obtained to their original ones.

Fig. 3 shows the sectional view of the mechanically modified structure. From the engine crank end on the left all the way to the right locates the extended ISG shaft, the encoder, the ISG rotor and the output shaft.

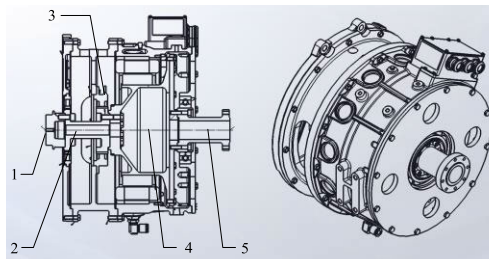


FIGURE 3. Mechanically modified structure. 1. Engine crank end, 2. Extended ISG shaft, 3. Encoder, 4. ISG motor, 5. Output shaft.

B. EXPERIMENTAL ENGINE AND MOTOR

The specifications of the engine are shown in Table 1. It is a 4 cylinder in-line diesel engine manufactured by Yuchai.

The parameters of the FISG are listed in Table 2. Its peak torque is 600 Nm. For safety and durability reasons, the torque demand in MCU is limited within ± 400 Nm, which is the rated torque of the motor.

The specifications of the battery system are listed in Table 3. It consists of two series-connected ternary-lithium-battery packs, which are manufactured by KeyPower.

C. SENSORS AND SIGNAL COLLECTING SYSTEM

The in-cylinder pressure signals are collected by PSG (pressure sensor glow-plug), which is a type of mass-produced

TABLE 1. Specifications of the engine.

Parameter	Description ^a
Engine model	YC4EG185
Ignition order	1-3-4-2
Idle speed (rpm)	650 \pm 25
Min fuel consumption rate (g/kWh)	198
Max torque/speed (Nm/rpm)	700/1300 to 1800
Rated power (kW)	136
Speed at rated power (rpm)	2500
Compression ratio	17.5
Displacement (L)	4.73
Crank radius (mm)	60
Connecting rod mass (kg)	2.291 \pm 0.1
Connecting rod length (mm)	187
Cylinder bore (mm)	112
Piston diameter (mm)	111.65
Offset of the piston pin (mm)	0.5 \pm 0.1
Piston mass (kg)	1.562 \pm 0.012

TABLE 2. Specifications of the motor.

Parameter	Description ^a
Motor model	TZ435XS-SL080F
Motor type	PMSM
Peak power (60s) (kW)	80 \pm 5%
Peak Torque (60s) (Nm)	600 \pm 5%
Rated torque/ speed (Nm/rpm)	400 \pm 5%/1275
Max no-load speed (rpm)	3000

piezoresistive pressure sensor integrated with a fast response glow plug. Its structure and main components are shown in Fig. 4. In-cylinder pressure information is needed when calculating the engine-out torque.

TABLE 3. Specifications of the battery system.

Parameter	Description ^a
Battery type	Ternary lithium
Nominal voltage (V)	503.7
Nominal capacity (Ah/kWh)	148/74.5
Peak discharge current (A)	450
Peak charge current (A)	300
Continuous discharge current (A)	150
Continuous charge current (A)	60 (Fast), 20 (slow)
Cooling method	Natural cooling

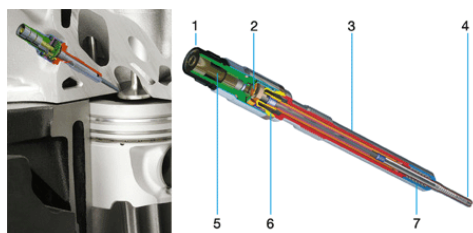


FIGURE 4. Components of the PSG: 1 - Plug, 2 - Circuit board with electronics, 3 - Glow plug body, 4 - Glow plug heating rod, 5 - High voltage connection, 6 - Measuring diaphragm, 7 - Gasket [25].

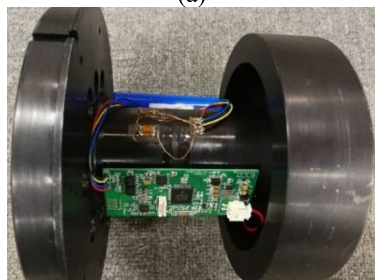
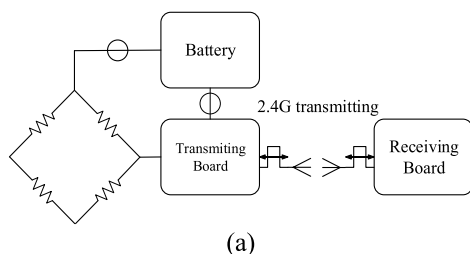


FIGURE 5. (a) is the block diagram of the strain sensor. (b) is the picture of the ready-to-use strain sensor. There are strain gauges attached onto the shaft. The PCB is responsible for data processing and data transmitting. The antenna of 2.4 GHz wireless data transfer can be observed.

In order to extract the shearing strain, which is linear to the torque, a Wheatstone Bridge is used. Four strain gauges are attached on the shaft surface next to each other, acting as 4 resistors in the Wheatstone Bridge. Since the shaft is rotating, a non-contact wireless signal transfer approach is adopted. A battery is also attached to the shaft for continuous power supply. Fig. 5 (a) shows its block diagram. The sampling rate of its analog-to-digital modular is 500 Msps. The bottle neck occurs at the wireless data transfer, whose frequency is 2.4 GHz. Through test, the maximum transfer

rate is over 6 Ksps, which takes about 0.17ms to update one value. For engine analysis, at 1000rpm, there still would be nearly 360 samples per round. Fig. 5 (b) shows the picture of the ready-to-use strain sensor.

An encoder is used to sample the angular position, from which the rotational speed and acceleration can be obtained. Its key technical parameters are listed in Table 4. The resolution is 2048 pulses per round, which is high enough for our research.

TABLE 4. Specifications of the encoder.

Parameter	Description ^a
Power supply (V)	DC 5±0.25
Encoder model	STS256T
Output type	Driver AM26C311
High level output voltage (V)	≥2.5
Low level output voltage (V)	≤0.5
Resolution	2048 P/r
Maximum speed (rpm)	5000

All signals are synchronized in a data logger named Saleae Logic Pro 16 logic analyzer. 4 channels for the analog inputs are used to capture the in-cylinder pressure signals. 2 channels for the digital inputs are used to record the encoder angle and the lap flag. 1 channel of CAN (controller area network) is used to communicate with the strain sensor. The digital and analog sample rates are set as 500 Msps and 5 Ksps respectively.

It should be noted that all the sensors introduced above in the signal collecting system are installed for the engine torque off-line calculation and experimental verification purposes. None of them are needed during the final online application of active damping.

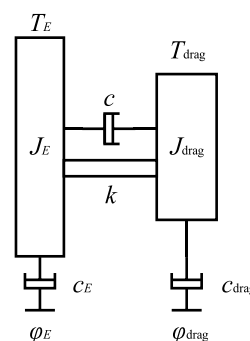


FIGURE 6. Dual-lumped-mass model of the Testbench.

IV. SIMULATION RESEARCH OF ACTIVE DAMPING

A. FEASIBILITY VALIDATION BASED ON ENGINE TORQUE OBSERVER

As shown in Fig. 6, the overall testbench is simplified as a dual-lumped-mass elastic model. The engine crank is represented as the lumped mass J_E on the left while the rest part of the testbench, including the rotors of the motor and

the dynamometer, is simplified as the lumped mass J_{drag} on the right. The connecting shaft is elastic with stiffness k and damp c . The angular crank position and the damp of each lumped mass are φ and c with the same footnotes as their moments of inertia. The torques exerting upon each lumped mass are T_E and T_{drag} respectively. The model is built to calculate the torque on the connecting shaft T_{target} .

The dynamical differential equation set drawn from the dual-lumped-mass model is organized as (1).

$$\begin{aligned} J_E \ddot{\varphi}_E &= T_E - \dot{\varphi}_E c_E - k(\varphi_E - \varphi_{drag}) - c(\dot{\varphi}_E - \dot{\varphi}_{drag}) \\ J_{drag} \ddot{\varphi}_{drag} &= T_{drag} - \dot{\varphi}_{drag} c_{drag} + k(\varphi_E - \varphi_{drag}) \\ &\quad + c(\dot{\varphi}_E - \dot{\varphi}_{drag}) \end{aligned} \quad (1)$$

The space-state variables can be defined as the vector (2).

$$x = [\varphi^T \quad \dot{\varphi}^T]^T = \begin{bmatrix} \varphi_E & \varphi_{drag} & \vdots & \dot{\varphi}_E & \dot{\varphi}_{drag} \end{bmatrix}^T \quad (2)$$

Then, equation (3) can be given as

$$\dot{J}x = Ax + T \quad (3)$$

where J, A and T can be given as (4), (5) and (6).

$$J = \begin{bmatrix} I & & & & \\ & J & & & \\ & & & & \\ & & & & \\ & & & & \end{bmatrix} = \begin{bmatrix} 1 & & & & \\ & 1 & & & \\ & & J_E & & \\ & & & & \\ & & & & J_{drag} \end{bmatrix} \quad (4)$$

$$\begin{aligned} A &= \begin{bmatrix} 0 & I \\ -K & -C \end{bmatrix} \\ &= \begin{bmatrix} 0_{2 \times 2} & & & I_{2 \times 2} & & \\ -k & k & -c_{drag} & -c & & c \\ k & -k & c & & -c_{drag} & -c \end{bmatrix} \end{aligned} \quad (5)$$

$$T = [0^T \quad \hat{T}^T]^T = [0 \quad 0 \quad T_E \quad T_{drag}]^T \quad (6)$$

Then, (1) can be reorganized as (7).

$$J\ddot{\varphi} + C\dot{\varphi} + K\varphi = \hat{T} = [T_E \quad T_{drag}]^T \quad (7)$$

The observer torque T_{target} can be obtained by solving (8). T_{target} is the torque on the shaft connecting the engine and the motor. It is also the ideal torque demand that the motor should follow to best reduce the speed variation.

$$J_E \ddot{\varphi}_E = T_E + T_{target} - c_E \dot{\varphi}_E \quad (8)$$

Which can also be given as (9).

$$T_{target} = J_E \ddot{\varphi}_E + c_E \dot{\varphi}_E - T_E \quad (9)$$

T_E consists of the gas torque, the reciprocating inertial torque due to the piston motion, and the torque from the reciprocating and the rotational lumped inertias of the connecting rod. Based on the energy conservation law, we can get (10).

$$\begin{aligned} T_g(\varphi) d\varphi &= p_g(\varphi) A_p ds \\ T_g(\varphi) &= p_g(\varphi) A_p \frac{ds}{d\varphi} \end{aligned} \quad (10)$$

where $T_g(\varphi)$ is the gas torque. $p_g(\varphi)$ is the in-cylinder pressure. s is the piston displacement and A_p is the area of the piston top surface. According to the mechanical structure of the crank-connecting-rod system, (11) can be obtained, where λ is the crank-to-connecting-rod ratio.

$$\frac{ds}{d\varphi} = r \left[\sin\varphi + \frac{\lambda}{2} \sin 2\varphi \right] \quad (11)$$

The connecting rod can be simplified as the dual-mass model, where the mass of the connecting rod is lumped on the piston pin and the crank pin, which are m_A and m_B . The total mass and the centroid position of the simplified model remains the same. While its moment of inertia, however, varies. If converting the reciprocating m_A to the rotational inertia about the crankshaft axis J_A , J_A is the function of the crank position.

$$J_A = J_A(\varphi) \quad (12)$$

The torque resulting from the reciprocating motion of m_A can be given as (13).

$$T_{MA}(\varphi) = -J_A(\varphi) \ddot{\varphi} - \frac{1}{2} \frac{dJ_A(\varphi)}{d\varphi} \dot{\varphi}^2 \quad (13)$$

The torque due to the equivalent mass m_B can be calculated by (14).

$$T_{MB}(\varphi) = -m_B r^2 \ddot{\varphi} \quad (14)$$

Therefore, the torque resulting from the connecting-rod motion can be expressed as (15).

$$\begin{aligned} T_m(\varphi) &= T_{MA}(\varphi) + T_{MB}(\varphi) \\ &= -\left(J_A(\varphi) + m_B r^2 \right) \ddot{\varphi} - \frac{1}{2} \frac{dJ_A(\varphi)}{d\varphi} \dot{\varphi}^2 \end{aligned} \quad (15)$$

The relationship between m_A and J_A can be derived from the energy conservation law as (16).

$$\frac{1}{2} J_A(\varphi) \left(\frac{d\varphi}{dt} \right)^2 = \frac{1}{2} m_A \left(\frac{ds}{dt} \right)^2 \quad (16)$$

So, J_A can be given as (17).

$$J_A(\varphi) = m_A \left(\frac{ds}{d\varphi} \right)^2 \quad (17)$$

Then,

$$\frac{dJ_A(\varphi)}{d\varphi} = \frac{d \left[m_A \left(\frac{ds}{d\varphi} \right)^2 \right]}{d\varphi} = 2m_A \frac{ds}{d\varphi} \frac{d^2s}{d\varphi^2} \quad (18)$$

where,

$$\frac{d^2s}{d\varphi^2} = r(\cos\varphi + \lambda \cos 2\varphi) \quad (19)$$

Similarly, for the torque due to the piston motion, $T_p(\varphi)$ can be obtained from the following equations.

$$T_p(\varphi) = -J_p(\varphi) \ddot{\varphi} - \frac{1}{2} \frac{dJ_p(\varphi)}{d\varphi} \dot{\varphi}^2 \quad (20)$$

$$J_p(\varphi) = m_p \left(\frac{ds}{d\varphi} \right)^2 \quad (21)$$

For a 4-cylinder engine, T_E can be calculated by (22).

$$T_E(\varphi) = \sum_{i=1}^4 T_i(\varphi) = \sum_{i=1}^4 [T_{g_i}(\varphi) + T_{m_i}(\varphi) + T_{p_i}(\varphi)] \quad (22)$$

The torque observer has been mathematically established as (9). The inputs are the $p_g(\varphi)$ of each cylinder and the crank signal. The output is the observer torque T_{target} , whose main component is the opposite-phase engine torque $-T_E$.

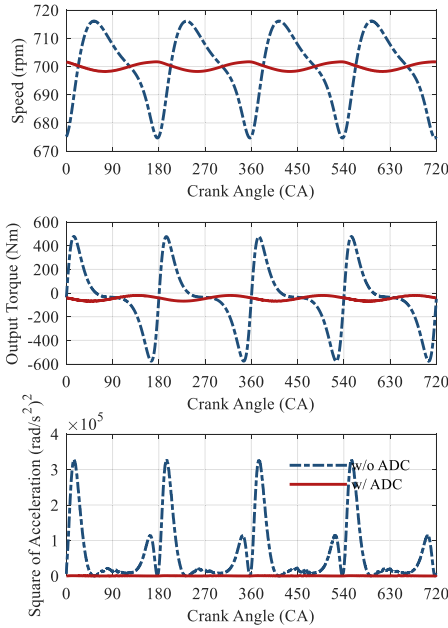


FIGURE 7. Active damping simulation results using the observer torque T_{target} .

Fig. 7 shows the active damping simulation results when letting motor generate the torque waveform T_{target} with the joint help of Matlab and AMESim. The blue curves are results without active damping. The red curves show the results with this algorithm. In the top two figures, the speed and the output torque vibration can be reduced effectively. In the last picture demonstrates a new indicator called the square of the angular acceleration, representing how much energy the vibration contains. With active damping, this indicator can also be reduced significantly. In conclusion, suppressing the crank vibration by active torque cancellation is theoretically feasible.

B. ONLINE APPLICATION ORIENTED TORQUE WAVEFORM FOR MOTOR

In this section, some realistic factors, including the motor response delay and its torque demand limit, are taken into consideration. Fig. 8 takes engine cranking at 700rpm for example, showing how to get the practical-application-oriented motor torque demand from T_{target} .

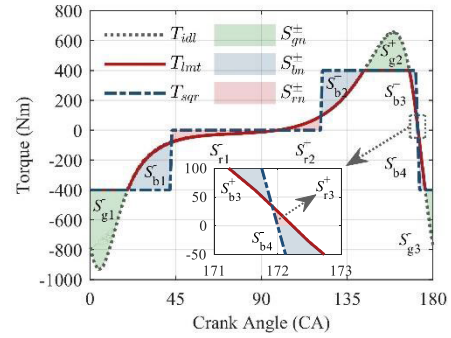


FIGURE 8. Online application oriented torque demand for motor.

To compensate the motor's response delay, the ideal torque waveform T_{idl} , represented as the grey dotted curve, is obtained by adding a differential module right after T_{target} in the simulated control system. Therefore, T_{idl} has a more advanced phase and a larger amplitude than T_{target} . Next, in MCU, the motor's torque demand is limited by ± 400 Nm, shown as the red solid waveform T_{lmt} . It is concluded in [11] that applying motor torque having the rectangular waveform is the most effective in reducing the driveline speed variation and can get the same damping performance with the smallest peak torque and the lowest energy loss level compared with the sine waveform and the opposite-phase engine torque. Finally, to realize a better damping level of the vibration with a compact motor, as in this research for a parallel hybrid powertrain, where the peak torque of the motor is limited by ± 400 Nm, the motor's target torque can be further simplified as the rectangular waveform T_{sqr} , shown as the blue dash-dot line in Fig. 8.

T_{sqr} can be obtained by solving the following optimization problem to get the optimal A , w and θ .

$$\text{Minimize } J = \alpha J_1 + \beta J_2 = J(A, w, \theta) \quad (23)$$

$$\text{Subject to } \begin{cases} \alpha + \beta = 1 \\ 0 \leq A \leq 400 \\ 0 < w \leq \frac{\pi}{2} \\ 0 \leq \theta \leq \pi \end{cases} \quad (24)$$

where A and w are the amplitude and the width of the square waveform. θ is the crank position where T_{sqr} crosses the free position of the crank (0° CA) from the positive end to the negative end. J_1 is defined as,

$$J_1 = \frac{\int_0^\pi |T_{idl}| d\varphi - \int_0^\pi |T_{sqr}| d\varphi}{\int_0^\pi |T_{idl}| d\varphi} = \frac{S_g + S_r - S_b}{\int_0^\pi |T_{idl}| d\varphi} \quad (25)$$

Which is the absolute mechanical work difference ratio between the absolute square wave torque T_{sqr} and the absolute ideal torque waveform T_{idl} . When taking J_1 as part of the cost function J , the total work done by the square wave torque T_{sqr} in both rotational directions can be close to that done by the

ideal torque waveform T_{idl} .

$$J_2 = \frac{\int_0^\pi |T_{lmt} - T_{sqr}| d\varphi}{\int_0^\pi |T_{lmt}| d\varphi} = \frac{S_r + S_b}{\int_0^\pi |T_{lmt}| d\varphi} \quad (26)$$

Besides, J_2 in the cost function J is defined to indicate how close are the phases of the square wave torque T_{sqr} and the limited torque demand T_{lmt} . To help clarify this issue more clearly, S_g , S_b and S_r are defined as the following equations, also illustrated as the colored blocks in Fig. 8.

$$\begin{cases} S_g = S_{g1}^- + S_{g2}^+ + S_{g3}^- \\ S_b = S_{b1}^- + S_{b2}^+ + S_{b3}^+ + S_{b4}^- \\ S_r = S_{r1}^- + S_{r2}^+ + S_{r3}^+ \end{cases} \quad (27)$$

In equation (23), α and β are used to balance J between J_1 and J_2 . When $\alpha = 1$, the work done by the motor will be sufficient but may be exerted at the wrong crank phase, probably resulting in an even larger vibration level. When $\beta = 1$, the work done by the motor would be exerted at the proper crank position, so the vibration would be damped but may not in the most effective way due to the insufficient motor power. In this paper, α and β are set to be 0.4 and 0.6. In this scenario, the optimal A , w and θ are calculated to be 400, 50 and 172 respectively. The active damping simulation results under different torque strategies using T_{lmt} and T_{sqr} respectively are shown in Figure 8.

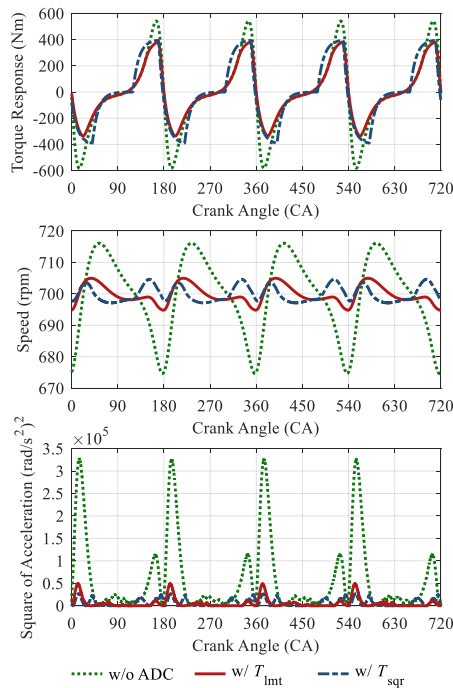


FIGURE 9. Active damping simulation under different torque strategies.

The top subfigure in Fig. 9 illustrates and compares the motor’s responses under T_{lmt} and T_{sqr} , presented in red solid curve and blue dash-dot curve respectively. Besides, the green dotted curve is the observer torque T_{target} , which should be

the ideal output torque of the motor. The lower two subfigures demonstrate two indicators, including the crank speed and the square of the angular acceleration, in conditions without active damping (green) as well as under two different torque strategies T_{lmt} and T_{sqr} (in red and blue). With realistic factors considered, the vibration amplitudes of the two indicators can still be effectively attenuated, indicating that both of the two motor torque demand waveforms are competent and can be used online. More specifically, the speed vibration range under the rectangular waveform T_{sqr} is slightly smaller than that under T_{lmt} . Therefore, the simplification of the T_{idl} is reasonable and the rectangular waveform T_{sqr} is adopted for online application.

V. RESOLVER-BASED CRANK POSITION REAL-TIME CALCULATION METHOD

A. ALGORITHM DESIGN

The real-time crank position must be known so that the motor can output crank-position-based torque ripples. One possible way is to let the engine control unit (ECU) send the crank position message to MCU via CAN. Once the MCU receives the message, the torque demand can be determined by looking up the crank-torque table. However, this method might still not work well because of the bad synchronization between MCU and ECU due to the lag in the CAN communication, which could be several milliseconds. Therefore, a real-time crank position calculation method with the help of the original resolver is proposed, which can be programmed directly in MCU. The crank position can be updated by the interval of the MCU’s single control cycle, which is 0.2 ms. No additional sensors or controllers are needed for the crank position calculation.



FIGURE 10. The stator and the rotor of the resolver.

Motor needs to know the real-time shaft position with the help of the resolver when generating the rotating magnetic field. As shown in Fig. 10. As for the experimental motor, it has 12 pole pairs. Therefore, its resolver rotor has 12 repeating waves. The output voltage of the resolver, which is represented as a 16-bit unsigned binary word, refers to a specific position on each wave. This unsigned binary word is defined as digital angular position. Here, 16-bit is the resolution of the resolver-to-digital converter. So, the range of the digital angular position is 0 to 65535. When the shaft

rotates by one revolution in certain direction, this parameter repeats from 0 to 65535 for 12 times.

The circumference is evenly divided by these 12 waves so that each wave refers to 30 °CA, which is defined as a crank step in Table 5. A new parameter named Counter is defined at MCU to be a counter, which is used to count how many complete waves (crank steps) have passed. For a four-stroke engine, a complete working cycle consists of 2 complete crank revolutions. Therefore, the counter would change from 0 to 23 within single working cycle, representing 24 crank steps that evenly divides the crank, whose range is from 0 to 720 °CA.

TABLE 5. Relationship between digital angle and crank position.

Digital angular position	0-2 ¹⁶ -1	0-2 ¹⁶ -1	...	0-2 ¹⁶ -1	0-2 ¹⁶ -1
DigAngPos					
Crank step					
CrankStep (CA)	0-30	0-30	...	0-30	0-30
Counter					
Counter	0	1	...	22	23
Crank Position (CA)					
CrankAbsPos	0-30	30-90	...	660-690	690-720

In conclusion, the real-time crank position can be calculated by the digital angular position and the counter with (28). The pending parameter k is the resolution of the resolver-to-digital converter, and p is the pole pair of the motor.

$$CrankAbsPos = \left(Counter + \frac{DigAngPos}{2^k} \right) \times \frac{360}{p} \quad (28)$$

B. REALIZATION AND DEMONSTRATION

The most essential part of the crank position calculation algorithm is to get the accurate counter, for which an algorithm is proposed. The revolutionary speed of the crank is defined as n (rpm) and the digital angular speed is represented as $DigAngVel$ (rpm). Their relationship can be established as (29) with the pole pair p .

$$DigAngVel = np \quad (29)$$

The duration of single MCU control cycle is defined as $CtrlCyc$ (μs). Cyclic digital angle Δ is defined as the variation of the digital angular position within one control cycle.

$$\Delta = \frac{2^k}{6 \times 10^7} \times DigAngVel \times CtrlCyc \quad (30)$$

1) STEP 1: BOUNDARY FOR COUNTER CHANGING

At MCU, the crank calculation algorithm is conducted during each control cycle. Therefore, the boundary, across which the counter should add or minus 1, must be a flexible range instead of a constant. The boundary range is defined as the cyclic digital angle Δ multiplied by coefficient Rit . Shown as the following.

If $DigAngPos(i - 1) \geq 2^k - Rit \times \Delta$ &
 $DigAngPos(i) \leq Rit \times \Delta$

$$Counter = Counter + 1$$

Elseif $DigAngPos(i - 1) \leq Rit \times \Delta$ & $DigAngPos(i) \geq 2^k - Rit \times \Delta$

$$Counter = Counter - 1$$

Else
End

There are several requirements the coefficient Rit must meet.

- i. In order to prevent the misjudgment caused by the signal glitch and noise, a margin must be added to Δ .

$$Rit > 1 \quad (31)$$

- ii. According to the range of the digital angular position $DigAngPos$, which is 0 to $2^k - 1$.

$$\begin{cases} 2^k - 1 \geq 2^k - Rit \times \Delta \geq 0 \\ 2^k - 1 \geq Rit \times \Delta \geq 0 \end{cases} \quad (32)$$

- iii. The judging conditions should be isolated from each other.

$$2^k - Rit \times \Delta > Rit \times \Delta \quad (33)$$

In summary, the coefficient Rit can be determined by the following inequality.

$$1 < Rit < \frac{3 \times 10^7}{n \times p \times CtrlCyc} \quad (34)$$

In our research, the pole pair of the motor p is 12. The control cycle of the MCU $CtrlCyc$ is 200 μs . At $n = 3000$ rpm, which is the highest cranking speed of the engine,

$$1 < Rit < 4.17 \quad (35)$$

In our research, coefficient Rit is set to be 2.

2) STEP 2: COUNTER DOUBLE CHECK AND MODIFICATION

The crank position cannot make step change because of its inertia. When there exists a gap, exceeding a certain criterion, between the calculated crank positions in the current and the former control cycles, the counter must be incorrect and should be modified. The mentioned criterion is defined as the crank step $CrankStep$ divided by coefficient α . Therefore, the following if-judgements are necessary.

If $abs [CrankAbsPos(i) - CrankAbsPos(i - 1)] \leq \frac{CrankStep}{\alpha}$
Elseif $CrankAbsPos(i) - CrankAbsPos(i - 1) > \frac{CrankStep}{\alpha}$

$$Counter = Counter - 1$$

Elseif $CrankAbsPos(i) - CrankAbsPos(i - 1) < -\frac{CrankStep}{\alpha}$

$$Counter = Counter + 1$$

End

Regarding the robustness of the algorithm, the criterion defined as the $CrankStep/\alpha$ should be smaller than $CrankStep$ to avoid misjudgment due to the signal noise. Meanwhile, the threshold should also be larger than the normal amount

of the crank position change within single control cycle to prevent misjudgment.

$$360 \times \frac{n}{60} \times \frac{CtrlCyc}{10^6} < \frac{CrankStep}{\alpha} < CrankStep \quad (36)$$

Similarly, the following inequality can be obtained with pending parameters by solving (36).

$$1 < \alpha < 8.33 \quad (37)$$

In our research, α is set to be 2. This step is the double check of the step 1. It is necessary for the robustness of the overall algorithm.

3) STEP 3: RANGE CHECK OF THE COUNTER

In this part, the *Counter* is limited within 0 to $0.5ps-1$. By the time the counter rises up beyond 23, it should fall back to 0. Also, when it falls below 0, it should turn into 23.

If $Counter > \frac{1}{2}ps - 1$

$$Counter = Counter - \frac{1}{2}ps$$

Elseif $Counter < 0$

$$Counter = Counter + \frac{1}{2}ps$$

Else

End

By the end of the step 3, the crank position can be calculated with the following formula.

$$CrankAbsPos(i) = \left[Counter + \frac{DigAngPos(i)}{2^k} \right] \times CrankStep \quad (38)$$

The overall MCU-embedded crank position calculation algorithm is summarized as the logic flow chart in Fig. 11.

This algorithm has been validated online. Note that this algorithm can be programmed directly in MCU. No extra controllers are needed for putting this algorithm into online application. Fig. 12 demonstrates how the parameters in this algorithm vary during the engine dragging and free deceleration.

The blue solid and the red dash-dot curves demonstrate how the counter and the crank position change. The green dash-dot curve is the crank speed and the grey dotted line shows part of the digital angular position. The digital angular position does not seem to be from 0 to 65535. This distortion results from the sampling rate, which is 10ms per sampling. Whereas the control cycle of the MCU is 200 μs . There exists no step-jumps in the crank position. All the other parameters change reasonably and accurately with no interruptions.

VI. RESULTS AND DISCUSSION

A. ACTIVE DAMPING IN STATIONARY OPERATING CONDITIONS

In this section, active damping is realized online. Fig. 13 shows the experimental results at 700rpm when the engine is cranking. The engine speed fluctuation range can be reduced

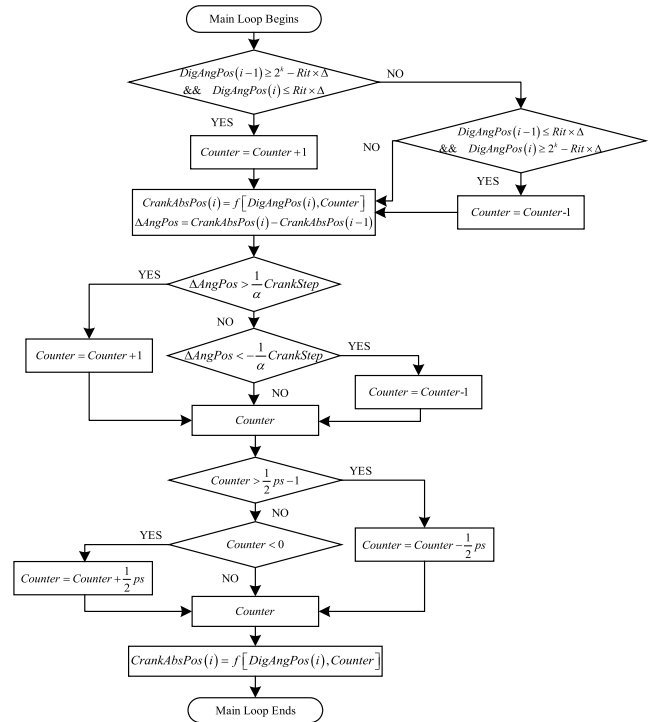


FIGURE 11. Diagram of the crank position calculation algorithm.

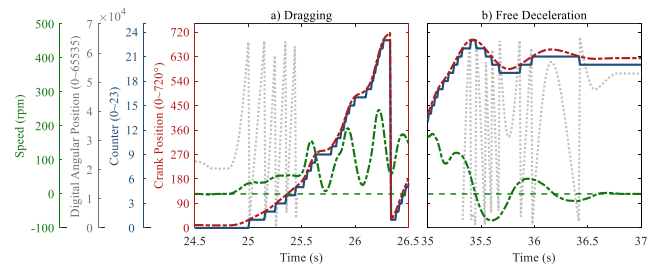


FIGURE 12. Parameters in MCU during the crank position calculation.

by active damping from 42.4 rpm to 8.6 rpm, whose reducing rate is 79.7%. The signal from the strain sensor has been normalized to the maximum positive output voltage. The normalized strain range on the output shaft can be suppressed by 64%. The cyclic squared angular acceleration is defined as the integral of the squared angular acceleration over a complete engine working cycle. This parameter is used to indicate the power of the vibration, which can be reduced by 89.7% by active damping.

Fig. 14 presents the frequency analysis of the driveline speed signal with and without active damping using FFT (fast Fourier transformation). Note that the harmonics corresponding to each frequency have been significantly attenuated.

This algorithm is also validated at different load from 0 Nm to 400 Nm and different speeds from 700 rpm to 1200 rpm. Active damping only needs to be activated at low engine speed because the natural filtering due to the rotor inertia, acting as a passive flywheel, is competent at high engine speed. Fig. 15 shows the range of the speed fluctuation with

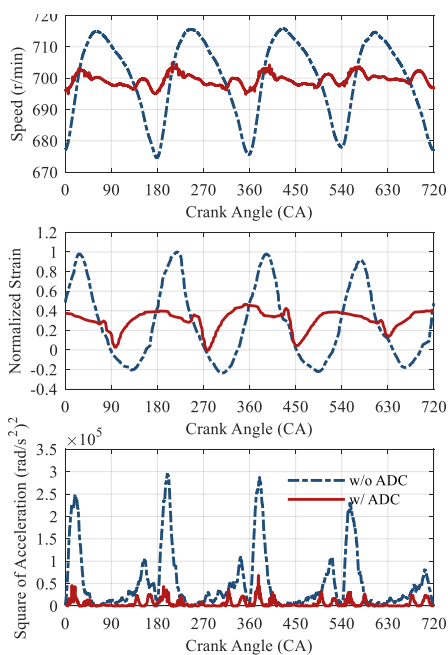


FIGURE 13. Active damping experiment results at 700rpm cranking.

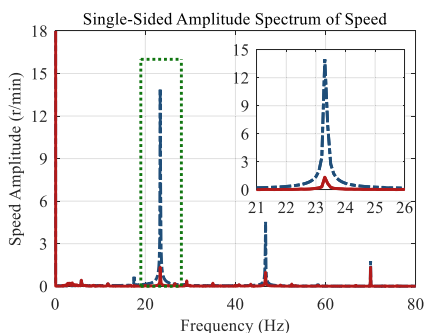


FIGURE 14. FFT analysis of the crank speed.

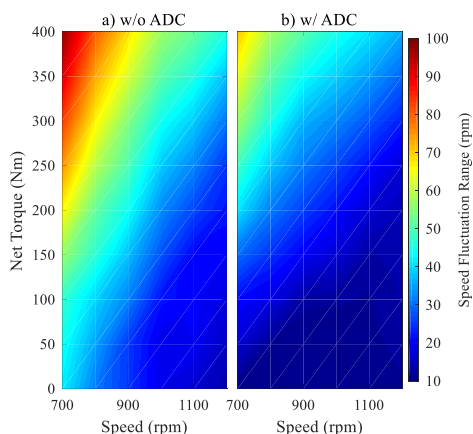


FIGURE 15. Speed fluctuation range w/ and w/o active damping.

and without active damping control. The color of the MAP indicates the speed fluctuation range, which is smaller at the point in cooler color. Each dot of the two MAPs uses the

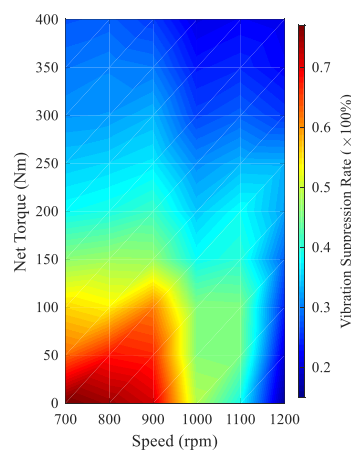


FIGURE 16. Reduction Rate of the speed fluctuation range.

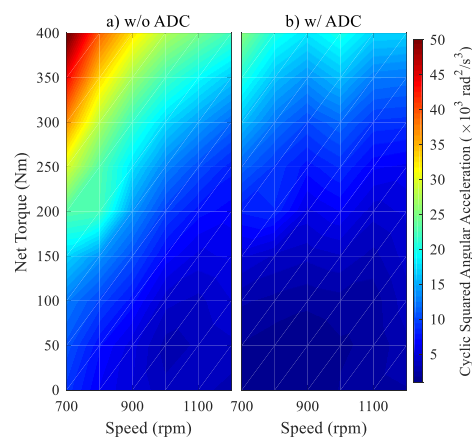


FIGURE 17. Cyclic squared angular acceleration w/ and w/o active damping.

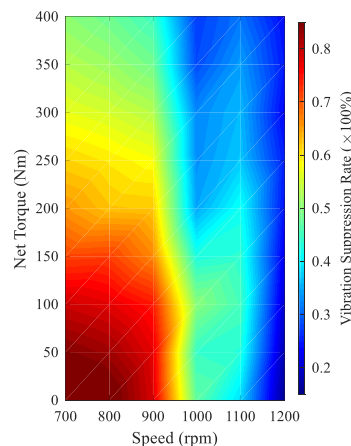


FIGURE 18. Reduction rate of the cyclic squared angular acceleration.

same control parameters, except for applying active damping or not. At higher engine speed, the speed fluctuation range is smaller, resulting from less time for the crank to accelerate or decelerate. At high load, the speed fluctuation range is larger due to the larger gas torque exerting on the crank.

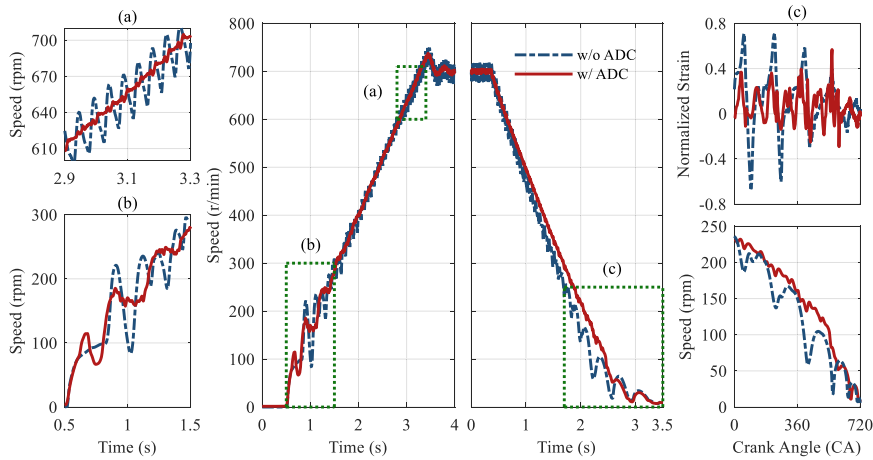


FIGURE 19. Active damping experimental results during engine dragging and free deceleration.

With active damping, the blue area can be greatly expanded, which indicates that the speed fluctuation can be suppressed effectively.

Fig. 16 shows the reducing rate of the speed fluctuation range after applying active damping. It can be concluded that this algorithm is more effective at low speed and load. At high speed, the speed fluctuation range is already small, which leaves barely no room for further improvement. At high load, its effectiveness is limited by the maximal motor output torque.

Fig. 17 shows the cyclic squared angular acceleration with and without active damping control. Similar with how the speed range changes, this indicator is larger at low speed and high load. With active damping, the blue area can be greatly expanded, meaning that the vibration power can be reduced effectively.

Fig. 18 shows the reducing rate of the cyclic squared angular acceleration after switching on active damping. Compared with the results of speed fluctuation, active damping is less sensitive to the load than the speed. This indicator is an energy indicator, which refers to the mean vibration power during a complete engine working cycle. Therefore, active damping control is the most effective at low speed and below medium load.

B. ACTIVE DAMPING IN TRANSIENT OPERATING CONDITIONS

This algorithm is also validated in transient working conditions, such as dragging and free deceleration, shown as Fig. 19. From subfigure (a), where the details in the green dot box (a) are amplified, the speed fluctuation during the dragging process can be greatly suppressed into nearly a slope. In subfigure (b), the speed fluctuation due to the resonance can also be attenuated. During the free deceleration, with active damping turned on, the speed fluctuation range can also be reduced. Because of their different decelerations, the results are plotted with the crank angle, instead of time, as the x axis in subfigure (c). Results show that the normalized

strain during the free deceleration can be reduced by active damping. In contrast to the situation without active damping, where the speed signal looks like repetitive waves, the speed curve under active damping looks much smoother.

The normalized strain and the squared angular acceleration during dragging with and without active damping are shown in Fig. 20. With active damping, these two indicators can be reduced significantly. Similar conclusions can also be drawn from the free deceleration experiment results.

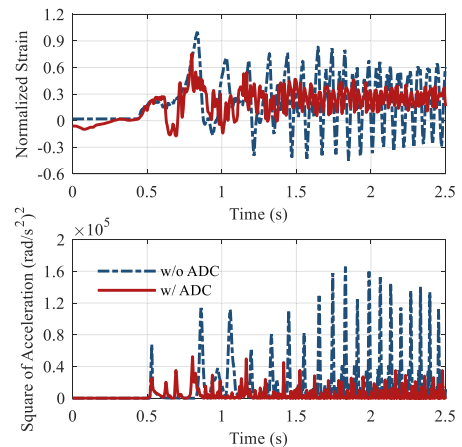


FIGURE 20. Active damping results during dragging.

In conclusion, the vibration during engine dragging and free deceleration can be attenuated effectively, which shows great potential to realize quick and quiet engine start and halt. In fact, this algorithm can also be applied to other typical transient conditions where the drivetrain's speed and load both vary.

VII. CONCLUSION AND OUTLOOK

Conclusions drawn from this research are summarized as:

- 1) The flywheel of the engine is replaced by the ISG rotor. There are no clutches or dampers either. The new hybrid system could be more light-weighted, more economical, more compact and have the potential to be

more reliable while maintaining or even improving its comfort.

- 2) A novel active damping method was proposed to reduce the driveline vibration by compensating the engine torque ripples with high-frequency motor torque pulsations. It is designed to be a feedforward method with the crank-torque look-up table directly programmed in MCU. The crank-torque table can be obtained by off-line simulation. Therefore, no extra sensors and controllers are needed when realizing active damping online.
- 3) An algorithm to calculate the real-time engine crank position with the help of the motor's original resolver was proposed and validated. It can also be programmed into MCU. Thus, no extra sensors or controllers are needed to get the real-time crank position.
- 4) Active damping was validated to be effective in both stationary and transient conditions, especially at low speed and below medium load. The cyclic squared angular acceleration can be reduced by 89.7% at 700 rpm cranking.

The electric energy consumption of the active damping needs future efforts. Comprehensive optimization considering both energy consumption and vibration attenuation is necessary. How active damping would change the in-cylinder combustion needs further exploration. When switching off individual cylinders for better fuel economy at partial load, comfort can be maintained or even enhanced using active damping control.

REFERENCES

- [1] H. K. Roy, A. McGordon, and P. A. Jennings, "A generalized powertrain design optimization methodology to reduce fuel economy variability in hybrid electric vehicles," *IEEE Trans. Veh. Technol.*, vol. 63, no. 3, pp. 1055–1070, Mar. 2014.
- [2] L. Li, S. You, C. Yang, B. Yan, J. Song, and Z. Chen, "Driving-behavior-aware stochastic model predictive control for plug-in hybrid electric buses," *Appl. Energy*, vol. 162, pp. 868–879, Jan. 2016.
- [3] O. Bitsche and G. Gutmann, "Systems for hybrid cars," *J. Power Sources*, vol. 127, nos. 1–2, pp. 8–15, Mar. 2004.
- [4] K. T. Chau and Y. S. Wong, "Overview of power management in hybrid electric vehicles," *Energy Convers. Manage.*, vol. 43, no. 15, pp. 1953–1968, Oct. 2002.
- [5] K. Govindswamy, T. Wellmann, and G. Eisele, "Aspects of NVH integration in hybrid vehicles," *SAE Int. J. Passenger Cars Mech. Syst.*, vol. 2, no. 1, pp. 1396–1405, May 2009.
- [6] G. Rizzoni, "Estimate of indicated torque from crankshaft speed fluctuations: A model for the dynamics of the IC engine," *IEEE Trans. Veh. Technol.*, vol. 38, no. 3, pp. 168–179, Aug. 1989.
- [7] J. Chauvin, G. Corde, P. Moulin, M. Castagné, N. Petit, and P. Rouchon, "Time-varying linear observer for torque balancing on a DI engine," *IFAC Proc. Volumes*, vol. 37, no. 22, pp. 137–142, Apr. 2004.
- [8] M. Nakamura, H. Hata, Y. Nakamura, T. Endo, and K. Iizuka, "Vibration reduction in rolling piston-type compressors through motor torque control. Basic study on theoretical analysis and computer simulation," *JSME Int. J. Vib., Control Eng., Ind.*, vol. 34, no. 2, pp. 200–209, 1991.
- [9] N. Mitsuru, H. Hiroaki, N. Yozoo, E. Tsunehiro, and I. Kenichi, "Study on vibration reduction of a rolling piston-type compressor by motor torque control: 1st report, Basic study on theoretical analysis and computer simulation," *Trans. Jpn. Soc. Mech. Eng. C*, vol. 56, no. 222, pp. 315–322, 1990.
- [10] Y. Kadomukai, M. Yamakado, Y. Nakamura, K. Murakami, and M. Fukushima, "Reducing vibration in idling vehicles by actively controlling electric machine torque," *JSME Int. J. C, Dyn., Control, Robot., Des. Manuf.*, vol. 38, no. 3, pp. 470–477, 1995.
- [11] Y. Nakajima, "A study on the reduction of crankshaft rotational vibration velocity by using a motor-generator," *JSAE Rev.*, vol. 21, no. 3, pp. 335–341, Jul. 2000.
- [12] S. V. Gusev, W. Johnson, and J. Miller, "Active flywheel control based on the method of moment restrictions," in *Proc. Amer. Control Conf.*, vol. 5, Jun. 1997, pp. 3426–3430.
- [13] K. P. Zeyen and T. Pels, "ISAD-A computer controlled integrated starter-alternator-damper-system," *SAE Trans.*, vol. 106, no. 3, pp. 2043–2053, Jan. 1997.
- [14] A. T. Zaremba, I. V. Burkov, and R. M. Stuntz, "Active damping of engine speed oscillations based on learning control," in *Proc. Amer. Control Conf. (ACC)*, Jun. 1998, pp. 2143–2147.
- [15] A. T. Zaremba and R. I. Davis, "Control design for active engine damping using a starter/alternator," in *Proc. Amer. Control Conf. (ACC)*, vol. 3, Jun. 2000, pp. 2043–2047.
- [16] R. D. Lorenz and R. I. Davis, "Apparatus and method for engine crankshaft torque ripple control in a hybrid electric vehicle," U.S. Patent 6336 070, Jan. 1, 2002.
- [17] R. I. Davis and R. D. Lorenz, "Engine torque ripple cancellation with an integrated starter alternator in a hybrid electric vehicle: Implementation and control," *IEEE Trans. Ind. Appl.*, vol. 39, no. 6, pp. 1765–1774, Nov. 2003.
- [18] P. Micheau and P. Coirault, "A harmonic controller of engine speed oscillations for hybrid vehicles," *IFAC Proc. Volumes*, vol. 38, no. 1, pp. 19–24, 2005.
- [19] M. Njeh, S. Cauet, and P. Coirault, "H ∞ control of combustion torque ripples on hybrid electric vehicles," *IFAC Proc. Volumes*, vol. 43, no. 7, pp. 542–547, Jul. 2010.
- [20] M. Njeh, S. Cauet, and P. Coirault, "LPV control of ICE torque ripple in hybrid electric vehicles," *IFAC Proc. Volumes*, vol. 44, no. 1, pp. 2931–2936, Jan. 2011.
- [21] S. Cauet, P. Coirault, and M. Njeh, "Diesel engine torque ripple reduction through LPV control in hybrid electric vehicle powertrain: Experimental results," *Control Eng. Pract.*, vol. 21, no. 12, pp. 1830–1840, Dec. 2013.
- [22] M. Beuschel and D. Schroder, "Identification and compensation of combustion torque pulsation using a harmonic activation neural network," in *Proc. 8th Eur. Conf. Power Electron. Appl. (EPE)*, 1999.
- [23] M. Beuschel, M. Rau, and D. Schroder, "Adaptive damping of torque pulsation using a starter generator-opportunities and boundaries," in *Proc. Conf. Rec. IEEE Ind. Appl. Conf. 35th IAS Annu. Meeting World Conf. Ind. Appl. Electr. Energy*, vol. 3, Oct. 2000, pp. 1403–1408.
- [24] R. S. Vadimalu and C. Beidl, "MPC for active torsional vibration reduction of hybrid electric powertrains," *IFAC-PapersOnLine*, vol. 49, no. 11, pp. 756–761, 2016.
- [25] (2014). *Pressure Sensor Glow Plug (PSG) for DIESEL Engines*. [Online]. Available: <http://www.beru.com/bw/products/diesel-cold-start-technology/pressure-sensor-glow-plug-psg>



YAODONG HU was born in Cangzhou, Hebei, China, in 1993. He received the B.S. degree in mechanical engineering from Tianjin University, in 2015. He is currently pursuing the Ph.D. degree with the Department of Automotive Engineering (DAE), Tsinghua University.

He gets involved in three national and inter-government Research and Development programs. He is the author of ten articles, seven patents, and two software copyrights. His research interests include advanced combustion concept and hybrid powertrain modeling and control.



FUYUAN YANG received the B.S. and M.S. degrees in internal combustion engine engineering and the Ph.D. degree from Tsinghua University, Beijing, China, in 1990, 1994, and 2005, respectively.

He is currently a Professor and the Deputy Head in education of the Department of Automotive Engineering, Tsinghua University. His research interests include advanced diesel engine, hybrid powertrain systems, and intelligent electric vehicle charging.



LEI DU was born in Huaiyuan, Anhui, China, in 1990. He received the B.S. degree in automotive engineering from Tsinghua University, Beijing, China, in 2012, where he is currently pursuing the Ph.D. degree with the Department of Automotive Engineering.

By applying Pontryagin minimum principle, he has worked out the optimal control of ISG torque to minimize the vibration. He is the author of nine articles and more than 30 inventions.

He proposed an index of vibration severity during engine start. His research interests include engine vibration analysis and optimal control.



JINYU ZHANG was born in Chengde, Hebei, China, in 1993. He received the B.S. degree in automotive engineering from Tsinghua University, Beijing, China, in 2016, where he is currently pursuing the Ph.D. degree with the Department of Automotive Engineering.

He is the author of two articles. His research interests include hybrid system control, especially motor control.



MINGGAO OUYANG received the Ph.D. degree in mechanical engineering from the Technical University of Denmark, Lyngby, Denmark, in 1993.

He is currently the Academician of Chinese Academy of Sciences, the Director of the State Key Laboratory of Automotive Safety and Energy, and the Cheung Kong Scholars Chair Professor with the Department of Automotive Engineering, Tsinghua University, Beijing, China. His main research interests include powertrain systems of energy-saving and new energy vehicles.

...